Isotopic effects in the structure of liquid methanol: II. Experimental data in Fourier space

2001 J. Phys.: Condens. Matter 13 11421

(http://iopscience.iop.org/0953-8984/13/50/302)

INSTITUTE OF PHYSICS PUBLISHING JOURNAL OF PHYSICS: CONDENSED MATTER

J. Phys.: Condens. Matter **13** (2001) 11421–11434 PII: S0953-8984(01)29582-4

Isotopic effects in the structure of liquid methanol: II. Experimental data in Fourier space

B Tomberli[1], P A Egelstaff[1], C J Benmore[2,3] and J Neuefeind[4]

[1] Department of Physics, University of Guelph, Guelph, Ontario, Canada N1G 2W1
[2] IPNS Division, Argonne National Laboratory, 9700 S. Cass Ave., Argonne, IL 60439, USA
[3] ISIS Facility, CLRC Rutherford Appleton Laboratory, Chilton, Oxon OX11 OXQ, UK
[4]Hamburger Synchrotronstrahlungslaboratorium HASYLAB at Deutsches Elektronensynchrotron DESY, Notkestr. 85, 22603 Hamburg, Germany

Received 10 October 2001
Published 30 November 2001
Online at stacks.iop.org/JPhysCM/13/11421

Abstract

The high-precision structural measurements of several methanol isotopes described in paper I are Fourier transformed to obtain their corresponding pair correlation functions. At room temperature we have observed a structural isotopic difference depending on the methanol isotopes used ranging between 2 and 5% at intramolecular distances and between 5 and 8% at intermolecular distances relative to the magnitude of $(g(r) - 1)$ for CH_3OH. For methanol at $-80\,^{\circ}C$, a maximum effect of 20% has been observed. All these effects may be explained in terms of changes in ground state librational motions and perturbations to the hydrogen bonding structure. The effects are compared with structural changes caused by temperature shifts and are shown to agree with the reciprocal space studies in paper I.

(Some figures in this article are in colour only in the electronic version)

1. Introduction and theoretical development

Contrary to the predictions of classical mechanics, the structures (and other equilibrium properties) of many (hydrogenous) liquids are known to be isotopically dependent [1–5]. In particular, our previous experiments have shown that carefully designed diffraction experiments using synchrotron radiation are a powerful tool for the determination of structural isotopic effects in hydrogenous liquids [6–8]. This paper is the second and final part of a study on such isotope effects in liquid methanol. The first part involved the background, experimental methods, and data reduction of methanol diffraction data collected by us and discussed in Q-space. This paper is an extension of those studies into real space. Therefore we begin with a brief synopsis of the methods used to Fourier transform the data from paper I.

Scattering of high-energy synchrotron radiation from a sample yields its electronic static structure factor, $S_X(Q)$ (see equation (3*b*) paper I). From this quantity, the electronic correlation function, $g_e(r)$ can be obtained via inverse Fourier transform

$$g_e(r) = 1 + \frac{1}{2\pi^2\rho r}\int Q\left(S_X(Q) - \sum_i f_i^2\right)\sin(Qr)\,\mathrm{d}Q \tag{1}$$

where ρ is the electronic density per Å^3 and $\sum_i f_i^2$ is the sum of the atomic form factors [9], f_i, over all the atoms in the molecule. Because of the near-sphericity of (especially the inner) electron shells in most atoms, it is possible to obtain approximately a nuclear correlation function by deconvoluting the electron cloud around each nucleus in r-space. Thus, using the molecular form factor, $(\Sigma f_i)^2$, one obtains the pseudonuclear intensity function

$$i(Q) = \frac{S_X(Q) - \sum_i f_i^2}{\left(\sum_i f_i\right)^2} \tag{2}$$

which can be inverse transformed to yield a molecular pseudonuclear correlation function in r-space:

$$g_X(r) = 1 + \frac{1}{2\pi^2\rho r}\int Qi(Q)\,\sin(Qr)\,\mathrm{d}Q \tag{3}$$

where ρ is the molecular density per Å^3. Here the X subscript indicates that the electronic structure factor was used to derive the correlation function and therefore the resulting total correlation function is composed of a sum of the atom–atom partial correlation functions with x-ray weightings (see equation (2) paper 1).

The isotopic difference between measurements on similar D and H compounds will be denoted by $\Delta g_e(r)$ and $\Delta g_X(r)$ for the electronic and pseudonuclear correlation functions respectively. Each difference, $\Delta S_X(Q)$ in Q-space, is computed and smoothed using maximum entropy techniques as described in paper I. The resulting smoothed isotopic difference is then Fourier transformed using the appropriate density and (if required) form factors

$$\Delta g_e(r) = \frac{1}{2\pi^2\rho r}\int Q\,\Delta S_X(Q)\,\sin(Qr)\,\mathrm{d}Q \tag{4}$$

$$\Delta g_X(r) = \frac{1}{2\pi^2\rho r}\int Q\Delta i(Q)\sin(Qr)\,\mathrm{d}Q$$

$$= \frac{1}{2\pi^2\rho r}\int Q\left(\frac{\Delta S_X(Q)}{\left(\sum_i f_i\right)^2}\right)\sin(Qr)\,\mathrm{d}Q. \tag{5}$$

In this case, the integrals were performed using a Simpson's rule quadrature over the selected range. Truncation effects were minimized by selecting the node in the integrand with the highest Q-value as the upper endpoint, Q_{MAX}, of the range. Q_{MAX} ranged between 16 and 18 Å^{-1}, depending on the isotopic difference used and similar truncation limits were used for the total structure and independent atom approximation (IAA) prediction of the intramolecular structure. The lower endpoint of the range was the first point in the smoothed data set, which was typically $Q_{\mathrm{MIN}} = 0.6$ Å^{-1}. The isotopic differences for $S(0)$ are very small and the extension of the integration range below Q_{MIN} to zero did not appreciably change the real space results. The correlation function was determined at the optimal $\mathrm{d}r = \pi/\Delta Q$ grid spacing, where $\Delta Q = Q_{\mathrm{MAX}} - Q_{\mathrm{MIN}}$. Smooth curves were then formed by joining the points with a cubic spline. The molecular factor of $\langle\Sigma f_i\rangle^{-2}$ present in $i(Q)$ (see equation (5) in paper 1) diminishes the weighting of the high-Q portion in the integrals of equations (1) and (2). No other modification function was employed upon the isotopic differences.

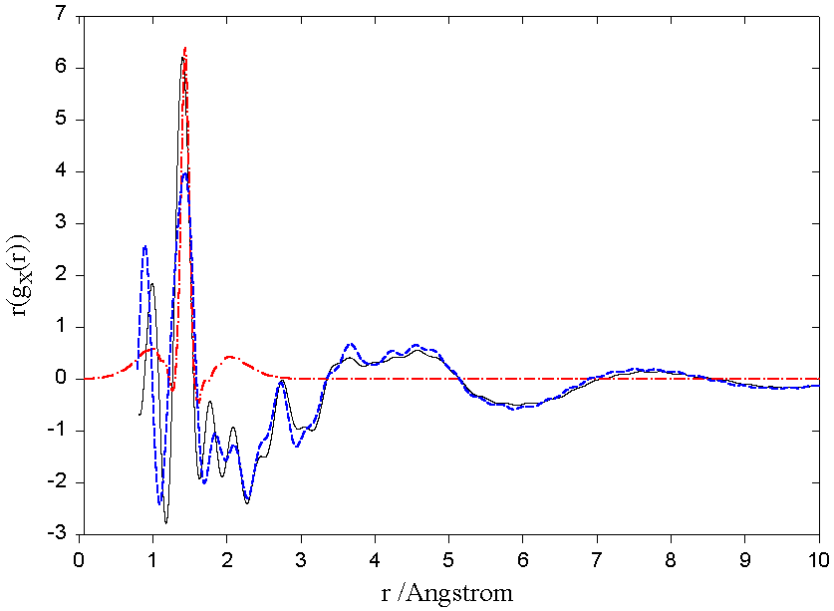

Figure 1. $r(g_X(r) - 1)$ CH_3OH at 24.5 °C (solid line) is compared to $r(g_X(r) - 1)$ at −80 °C (dashed line) and the intramolecular structure predicted from the IAA (dash-dot line) multiplied by the distance r.

The isotopic differences will be compared with $(g_X(r) - 1)$ for CH_3OH divided by an appropriate factor. The $g_X(r)$ data were not smoothed using the maximum entropy procedure used on the differences because it produced poorer agreement with the low r structure. Instead, a modified version of a previously developed convolution method [8] was used to smooth $g(r)$ for each isotope. This method broadens the measured $S(Q)$ by convoluting each point (as if they were delta functions in Q-space) with a Gaussian of width σ, to smear out the structure. To take into account varying statistical noise across the measured spectra, σ is varied as a function of Q:

$$S_{\text{smooth}}(Q) = S_{\text{measured}}(Q) \otimes \left(2\pi\sigma^2(Q)\right)^{-0.5} \exp -\frac{(Q - Q_O)^2}{2\sigma(Q)^2} \tag{6}$$

where $\otimes$ means a convolution. For this data set we defined

$$\sigma(Q) = \frac{\Delta Q}{2} A Q^2 + B \tag{7}$$

where ΔQ is the Q-spacing of the measured data. A and B are adjusted for the degree of smoothing required, depending on the quality of the data. For all the data presented in this work, A and B were of the order of unity.

The final data sets resulting from the above procedure were transformed to yield the total r-space structure curves shown in all the figures.

2. Total structure for CH_3OH at room temperature and −80 °C

In figure 1 our pseudonuclear curves (as given by equation (3)) for $g_X(r)$ of CH_3OH at 24.5 and −80 °C are compared with the predicted intramolecular structure from the IAA. The intramolecular results are obtained by a Fourier transform of the result from equation (5) of

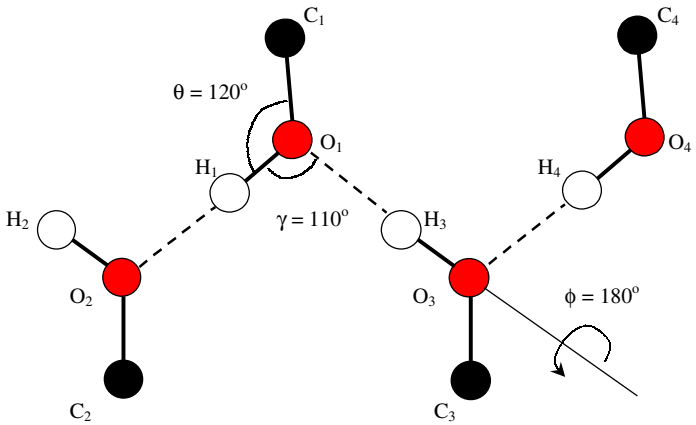

Figure 2. Schematic illustration of crystalline methanol structure with approximate distances: O_1–O_2 = 2.8 Å, H_1–O_2 = 1.8 Å, O_1–C_2 = 3.75 Å, O_2–O_3 = 4.6 Å, C_1–C_2 = 4.9 Å.

paper I using r_{CO} from table 3 of paper I and the remaining intramolecular parameters from table1 of paper I. At both temperatures for methanol, the 1.42 Å r_{CO} distance shows up as a clear peak in our data, which is approximately matched by the independent atom model. As expected, the area under this peak is shown to be relatively insensitive to the temperature. The $-80\,^{\circ}$C peak is broader due to poor experimental statistics in the high-Q portion of that data. At other intramolecular distances the agreement of the IAA with our measured result is not as good due to the fact that other intramolecular distances and bond angles were not fitted against our results. Nonetheless, there is qualitative agreement for $r < 2.0$ Å beyond which the IAA shows no distinct intramolecular correlations. At both temperatures a strong feature is visible near 1.0 Å which corresponds to the bonded C–H and O–H distances. The two data sets also do not agree well for $r < 1$ Å, probably due to insufficient counting statistics in the high-Q portion of the $-80\,^{\circ}$C data set.

There are two small peaks near $r = 2.0$ Å whose height and distance suggest that they involve {carbon–hydroxyl H} or {oxygen–methyl H} distances. These distances vary according to the twist angle between the OH and CH_3 group within a given molecule. At higher temperatures more configurations are thermodynamically accessible to the molecule and this could cause the observed differences for 1.5 Å $< r <$ 3.0 Å between the $-80\,^{\circ}$C and the 24.5 °C data. The ∼1.8 Å peak could instead be due to the predicted H-bonding O–H nearest neighbour. However, it is very likely that the 1.8 Å O–H intermolecular peak is too weak to be seen.

At intermolecular distances ($r > 3.0$ Å) the -80°C structure is slightly sharper than the 23.5 °C structure. The peak near 2.8 Å, attributed to the nearest-neighbour O–O distance [10] shows minor differences. Liquid methanol is believed to form winding hydrogen bonding chains similar to those in the crystalline state [10, 11]. In figure 2 we show the crystalline structure for comparison to our liquid state correlation function. Using figure 2 as a guide, we see that the broad peak visible in $(g_X(r) - 1)$ over 3.5 Å $< r <$ 4.8 Å at both temperatures is dominated by intermolecular carbon–oxygen interactions (e.g. O_1–C_2, O_2–O_3, C_1–C_2 in figure 2). Nearest neighbour correlations involving a single hydrogen may contribute to the broadness of the peak (e.g. O_1–C_2, C_1–H_2 and O_1–H_4). The small peaks visible in the broad hump over this range in the $-80\,^{\circ}$C liquid indicate that there is more rigidity in the chains at this temperature (that is there is less variation in the $O_2O_1O_3$ angle) than at room temperature.

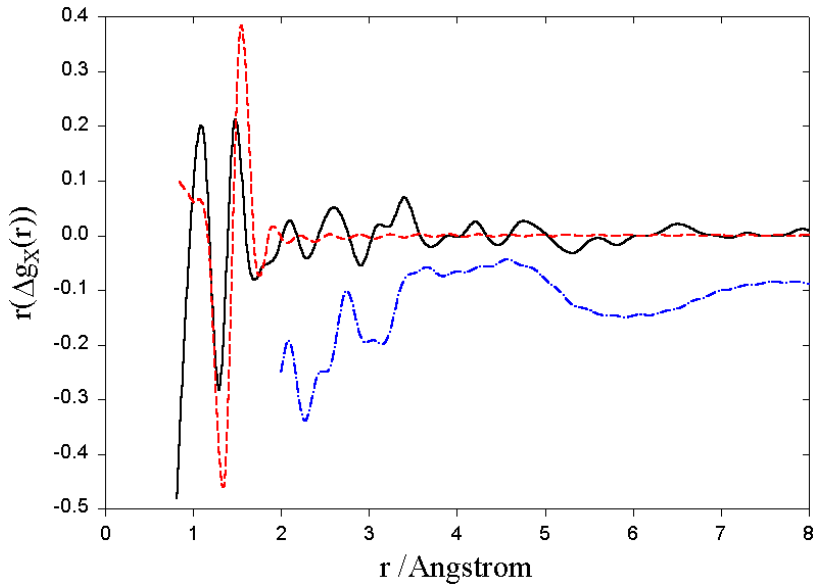

Figure 3. Pseudonuclear isotopic difference CD_3OH–CH_3OD at 23.5 °C (solid line) and the intramolecular isotopic difference predicted from the IAA (dashed line) are compared to $(g_X(r) - 1)/10$ at 23.5 °C displaced by −0.1 units (dash-dot line).

The next-nearest-neighbour O_2–O_3 correlation at $r = 4.6$ Å (assuming tetrahedral 109.5° O–O–O intermolecular bond angle in a zig-zag chain) and nearest-neighbour C_1–C_2 correlations (4.9 Å) are also visible at both temperatures. At room temperature, these correlations are weaker. However, at −80 °C two small peaks and a shoulder become visible. This is due to a combination of the increasing length of the average hydrogen-bonded chain and the decreased intermolecular motions as the temperature is decreased. There is a broad weak feature over 7–9 Å which is less sensitive to temperature variation and due to a combination of next-nearest-neighbour C–O correlations and third-nearest-neighbour O–O correlations along the chain in figure 2.

Comparison of the methanol structure in figure 1 with other liquids such as water [6] and benzene [8] shows that methanol structure lies in between these two liquids with regard to the ratio between the strength of the intermolecular and intramolecular correlations. Benzene has very small intermolecular correlations. Methanol has more significant correlations though they are smaller than those in water which has the strongest. This is clearly related to the amount of hydrogen bonding in each liquid. Benzene, dominated by weaker quadrupolar effects, has no hydrogen bonding and the least intermolecular structure. It is known that different motions are responsible for different isotopic effects [12]. The shift of the triple point to higher temperature (in heavy water) is a net effect: lower zero-point energies for deuterated water clusters raise the melting point whereas vibrational frequencies for deuterated species lower the melting point. In methanol the opportunity exists to separate effects due to methyl substitution, which are postulated to primarily affect the molecular librations, and effects due to hydroxyl substitution which are postulated to perturb the winding hydrogen chain structure.

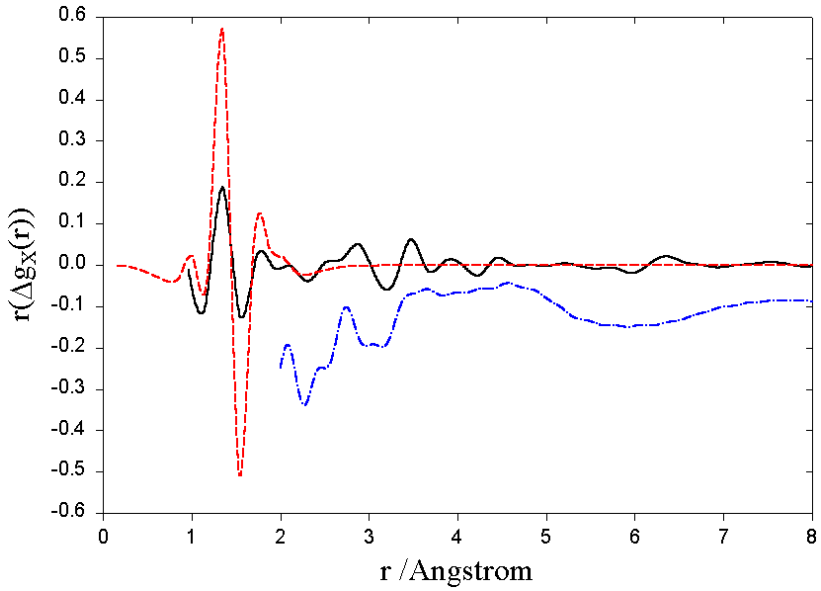

Figure 4. Pseudonuclear isotopic difference CD_3OD–CH_3OH at 23.5 °C (solid line) and the intramolecular isotopic difference predicted from the IAA (dashed line) are compared to $(g_X(r) - 1)/10$ at 23.5 °C displaced by −0.1 units (dash-dot line).

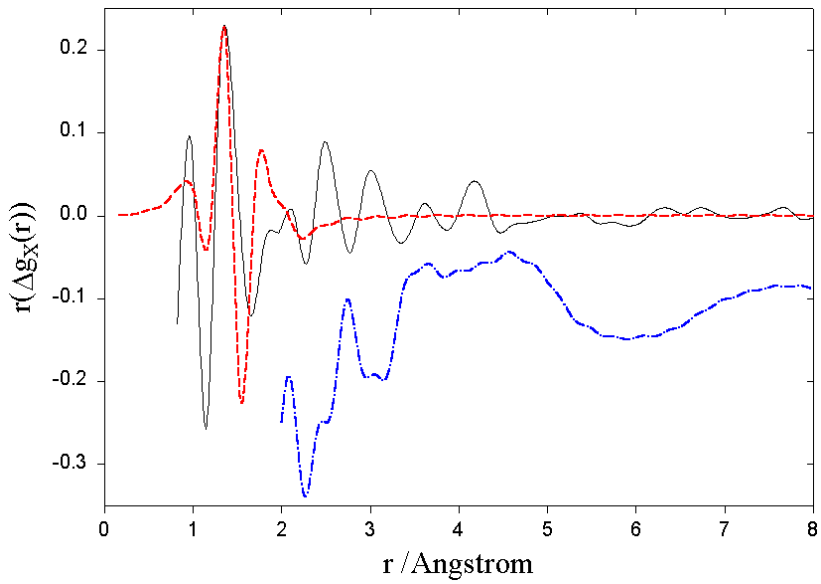

Figure 5. Pseudonuclear isotopic difference CD_3OH–CH_3OH at 23.5 °C (solid line) and the intramolecular isotopic difference predicted from the IAA (dashed line) are compared to $(g_X(r) - 1)/10$ at 23.5 °C displaced by −0.1 units (dash-dot line).

3. Isotopic differences in room temperature methanol

Figures 3–8 compare the Fourier transforms, $\Delta g_X(r)$, of the six room temperature isotopic differences, $\Delta S_X(Q)$, measured in part I, to predicted differences in the intramolecular structure

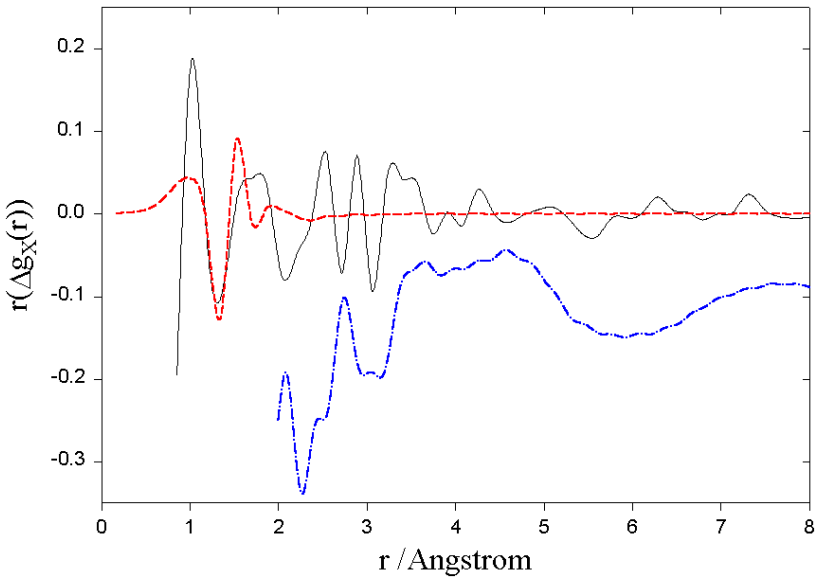

Figure 6. Pseudonuclear isotopic difference CD_3OD–CH_3OD at 23.5 °C (solid line) and the intramolecular isotopic difference predicted from the IAA (dashed line) are compared to $(g_X(r) - 1)/10$ at 23.5 °C displaced by −0.1 units (dash-dot line).

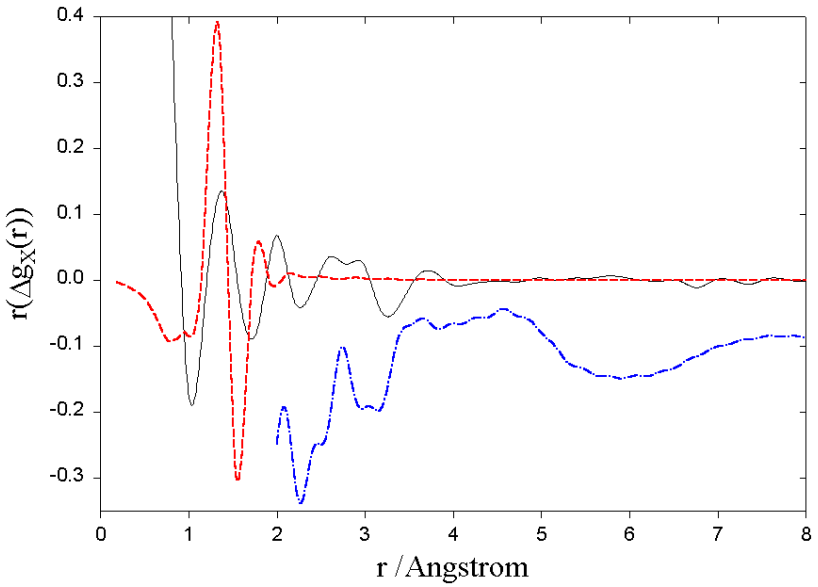

Figure 7. Pseudonuclear isotopic difference CH_3OD–CH_3OH at 23.5 °C (solid line) and the intramolecular isotopic difference predicted from the IAA (dashed line) are compared to $(g_X(r) - 1)/10$ at 23.5 °C displaced by −0.1 units (dash-dot line).

and to the total structure $(g_X(r) - 1)$ in liquid CH_3OH. Comparing figure 1 to figures 3–8, we see that the intramolecular ($r < 2.2$ Å) isotopic difference is about four to five percent of the total structure for CH_3OH. Several features are common to all of these figures. Firstly, the difference intramolecular structure, especially near $r = 1.5$ Å is qualitatively predicted by the

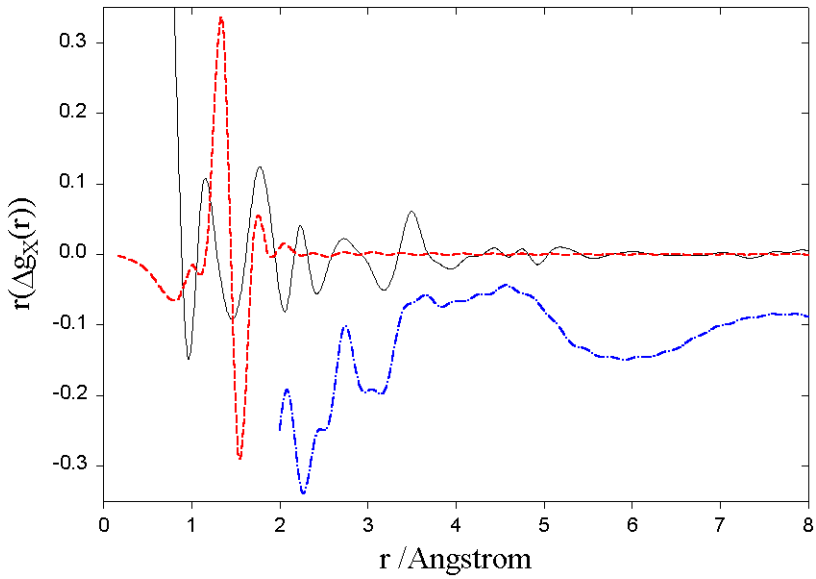

Figure 8. Pseudonuclear isotopic difference CD_3OD–CD_3OH at 23.5 °C (solid line) and the intramolecular isotopic difference predicted from the IAA (dashed line) are compared to $(g_X(r) - 1)/10$ at 23.5 °C displaced by −0.1 units (dash-dot line).

IAA. This is a result of the fitting of the C–O intramolecular bond length, r_{CO}, for each isotope in part I. Secondly, at intramolecular distances ($r > 2.5$ Å) the size of the isotope effect relative to the total structure is larger, in places on the order of ten percent. Lastly, from these figures we see a high degree of consistency between substitutions of the same type. For example, both of the methyl substitutions (figures 5 and 6) produce a dip at 2.8 Å which is flanked by peaks on either side, while both of the hydroxyl substitutions (figures 7 and 8) have broadened peaks which overlap at this distance. The double substitutions differ from each another over this range because figure 4 (CD_3OD–CH_3OH) has D to H substitution at both sites whereas figure 3 (CD_3OH–CH_3OD) has D to H substitution at the methyl site and H to D substitution at the hydroxyl site.

Figure 3 compares the CD_3OH–CH_3OD difference to the intramolecular difference predicted from the IAA and to the total structure for CH_3OH. For $0.8 < r < 2.5$ Å the agreement between the IAA prediction and our measured results are within about 30% of each other. The peak near 1.0 Å is caused by the decreased vibrations in the methyl D–C intramolecular distance compared with the methyl H–C. The shape near $r = 1.5$ Å is characteristic of the longer intramolecular CO bond in CD_3OH as compared with CH_3OD. This agrees with the Q-space measurements of paper I where r_{CO} for CD_3OH was indeed found to be longer than that of CH_3OD in table 3. The oscillations in the isotopic difference are about 3% as large as the oscillations in the total structure.

At intermolecular distances there is a nearly antisymmetric oscillation at 2.8 Å, very near the O–O nearest-neighbour distance, indicating that the CD_3OH isotope has more intensity at shorter distances and less at longer distances than the CH_3OD isotope. That is, the O–O distance (and by inference the H-bond) is shorter in CD_3OH. There is a peak near 3.4 Å which could be the result of the carbon atom attached to the oxygen atom moving in as the nearest-neighbour hydrogen bond is shortened. The small peaks between 4–5 Å are difficult to interpret. They may be due to next nearest neighbour correlations of oxygen or nearest-

neighbour carbon correlations because of their position. They are within the broad feature in the total structure in this region and therefore are probably due to sharpening in the structure of CD_3OH due to its decreased zero-point librational motions caused by its increased mass compared to CH_3OD.

Figure 4 compares the CD_3OD–CH_3OH difference to the intramolecular difference predicted from the IAA and to the total structure for CH_3OH. For $0.8 < r < 2.5$ there is qualitative agreement between the IAA prediction and our measured results. However, in this region the size of the IAA oscillations is greater by a factor of nearly three. This is an artifact caused by the maximum entropy procedure used to smooth the data. The smoothing causes this by damping the (in this case larger) oscillations in the isotopic difference at high Q. The $\langle F^2 \rangle$ fits to obtain the r_{CO} value used in the IAA calculation were performed on unsmoothed $Q(S_X(Q) - \Sigma f_i^2)/(\Sigma f_i)^2$ data for each isotope and therefore did not experience any such damping. Again there is a peak near 1.0 Å and the oscillations in the isotopic difference are about 3–4% as large as the oscillations in the total structure. There is a dip near 3.2 Å which is exactly between the 2.8 Å O–O nearest-neighbour distance and the 3.6 Å nearest-neighbour O–C distance. The interstitial region is depopulated in CD_3OD. In other words, the bonded regions are slightly sharper in CD_3OD. CD_3OD has more intensity at slightly longer distances than 2.8 Å, which suggests that the hydrogen bond is shorter in CH_3OH than CD_3OD. The peak near 3.3 Å could be due to a rotation of the nearest-neighbour CO axis in the plane of the winding chain structure. In this case, there is a combination of increased librational motion effects with perturbation to the hydrogen bonding chain structure. The small peaks near 3.8 and 4.5 Å are also consistent with a combination of increased librational motion and slight perturbations in the next-nearest-neighbour bond lengths.

Figure 5 compares the CD_3OH–CH_3OH methyl substitution difference to the intramolecular difference predicted from the IAA and to the total structure for CH_3OH. Unlike previous figures, in this figure there is no significant mixing of hydroxyl and methyl substitution effects. For $0.8 \text{ Å} < r < 2.5 \text{ Å}$ there is better agreement between the IAA prediction and our measured results. The peak at 1.45 Å agrees well with that of the IAA model and is due to changes at the intramolecular CO bond. Once more the oscillations in the intramolecular portion of the isotopic difference are about 4% as large as the oscillations in the total structure.

Intermolecularly, there is a sharp dip exactly at the 2.8 Å O–O nearest-neighbour distance with a characteristic shape indicating that the structural peak for CD_3OH is broader than CH_3OH: this effect is relatively large. The scale in figure 5 shows that it is about 10% of the total structure in $g(r)$ at 2.8 Å. This suggests that methyl hydrogens have an effect upon hydrogen bonding. In paper I this isotopic difference in Q-space was shown to correspond to cooling, which suggests that under these conditions these H-bonds broaden as they cool. Later we will see that the opposite behaviour occurs in this region with hydroxyl substitutions. Another possible contribution to the structure over the range $2.0 \text{ Å} < r < 3.7 \text{ Å}$ could be the intramolecular hydrogen–hydrogen correlations (which occur at 2.45 and 3 Å). However, hydrogen form factors are too weak to produce the observed peaks. A dip near 3.9 Å (that is qualitatively very similar to the one at 2.8 Å) can be attributed to decreased variation of the intermolecular OC (O_1–C_2 in figure 2) distance in CH_3OH, which is strongly coupled with the decreased O–O motions in CH_3OH compared with CD_3OH.

Figure 6 compares the CD_3OD–CH_3OD methyl substitution difference with the intramolecular difference predicted from the IAA and with the total structure for CH_3OH. The sharp peak near 1.0 Å indicates that the Debye–Waller factor is reduced in the C–methyl D intramolecular bond for CD_3OD due to the increased mass. The fact that this peak is sharper in our measured result than in the predicted IAA curve has two possible causes: (1) the difference in DW factors cited in table 1 of paper 1 for these bonds is too small (in fact, a much

bigger isotopic difference in DW factors than that shown in table 1 is required to reproduce the experimental results), (2) accumulated statistical errors at high Q decrease the accuracy of the transformed data at low r. There is a stronger peak near 3.2–3.4 Å which suggests that the O_1–C_2 distance (see figure 2) has shortened in this difference while it did not for CD_3OH–CH_3OH. Given that features near the O_1–O_2 distance are similar in both figures this suggests there is a slightly lower O_1–O_2–C_2 bond angle for CH_3OD than CD_3OD. The feature at 2.8 Å is considerably sharper as well. In general, this figure supports the conclusions for methyl substitution from figure 5.

Figures 7 and 8 compare the CH_3OD–CH_3OH and CD_3OD–CD_3OH hydroxyl substitution differences respectively with their intramolecular differences predicted from the IAA and with the total structure for CH_3OH. In these two cases, the IAA prediction of the intramolecular structure is poor. The magnitude of the measured effect is about 2–3% whereas the predicted effect is about 5 or 6% of the total intramolecular structure. This may be due to inadequacies of the IAA and imperfect knowledge of isotopic values for bond lengths. It is also partially due to the fact that the minimum intermolecular distance (O_1–H_2) is about 1.8 Å and therefore there may be some intermolecular correlations present at these distances which would not be predicted by the IAA. The shape of the measured difference is consistent with the measured decrease of about 0.15 Å in r_{CO} upon deuteration of the hydroxyl site (from table 3 of paper I). There is a strong dip near 1.0 Å due to broadening of the OD compared with OH bond. Because only one intramolecular (O_1–H_1) distance is affected (as opposed to three or four in the previous cases) the change in length and Debye–Waller factor must be large to produce such a significant dip in the isotopic difference. This effect was not modelled and therefore poorly reproduced by the IAA.

Intermolecularly, both figures 7 and 8 show clear peaks centred at 2.8 and 3.7 Å which can be attributed to the increased sharpness of the O–O intermolecular distances (and their strongly coupled associated carbons) in the hydrogenous isotope. This behaviour of the hydroxyl substitution is opposite to that for methyl substitution and was shown in paper 1 (table 4) to correspond to the deuterated isotope being effectively 4 °C hotter than the hydrogenous one. It suggests that the O–O distances sharpen as they heat up, a counterintuitive result which is supported by the cooling-induced broadening of the same feature seen in figures 5 and 6. The effect is again smaller than the methyl and double substitution effect, perhaps by about 4 or 5%. However, on a per hydrogen basis, the effect is relatively larger.

4. Isotopic differences in methanol at low temperatures

Five of the six isotopic differences from section 2 were also measured at a temperature of −80 °C. These measurements were taken at HASYLAB over two runs in 1999 and 2000. The CD_3OD–CH_3OD difference was not measured at −80 °C due to a shortage of machine time. The results of the remaining differences are summarized in figures 9 and 10. By comparison with figures 3–8, we see that the methyl substitution effect for $r < 2.5$ Å^{-1} is about the same size; about 4–5%. For $r > 2.5$ Å the effects are considerably larger and range from 10 to 20% of $g(r) - 1$.

Figure 9 compares the pseudonuclear differences CD_3OD–CH_3OH and CD_3OH–CH_3OH to each other and to $g(r) - 1$ for CH_3OH at −80 °C. The two differences agree very well for $r < 2.5$ suggesting that the agreement seen in Q-space in figure 5 of paper I between these curves was dominated by similarities in the isotopic differences at intramolecular distances. The interpretation is exactly the same as for the corresponding difference at room temperature. A combination of decreased Debye–Waller factors and changed r_{CO} distances is sufficient to explain the observed isotopic differences for $r < 2.5$ Å.

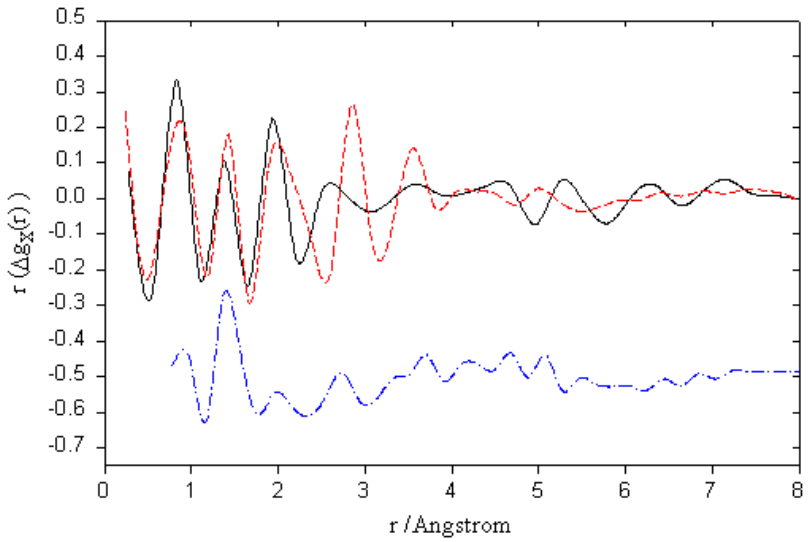

Figure 9. Pseudonuclear isotopic differences CD_3OD–CH_3OH (solid line) and CD_3OH–CH_3OH (dashed line) at $-80\,^{\circ}C$ are compared to $(g_X(r) - 1)/10$ at $-80\,^{\circ}C$ displaced by -0.4 units (dashed-dot line).

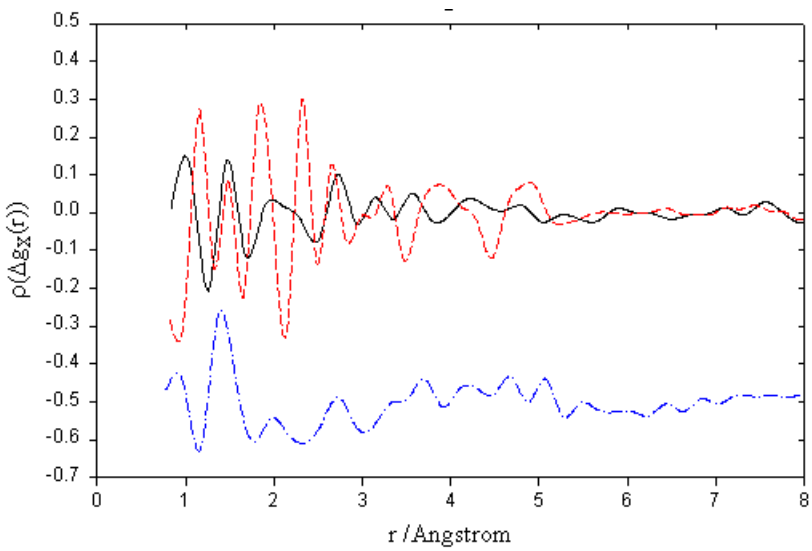

Figure 10. Pseudonuclear isotopic differences (solid line) CH_3OD–CH_3OH and CD_3OD–CD_3OH (dashed line) at $-80\,^{\circ}C$ are compared to $(g_X(r)-1)/10$ at $-80\,^{\circ}C$ displaced by -0.4 units (dashed-dot line).

Plotted in this fashion the CD_3OH–CH_3OD difference at $-80\,^{\circ}C$ (not shown) did not agree well with the two differences shown in figure 9 even though in Q-space all three curves were similar. If these curves are transformed using equation (4) to generate the electronic structure, then all three differences agree quite well for 2.5 Å $< r <$ 10 Å.

At intermolecular distances, the CD_3OH–CH_3OH difference is particularly large—about 25% of $g(r) - 1$. At room temperature a strong symmetric dip was observed at $r \sim 2.8$ Å

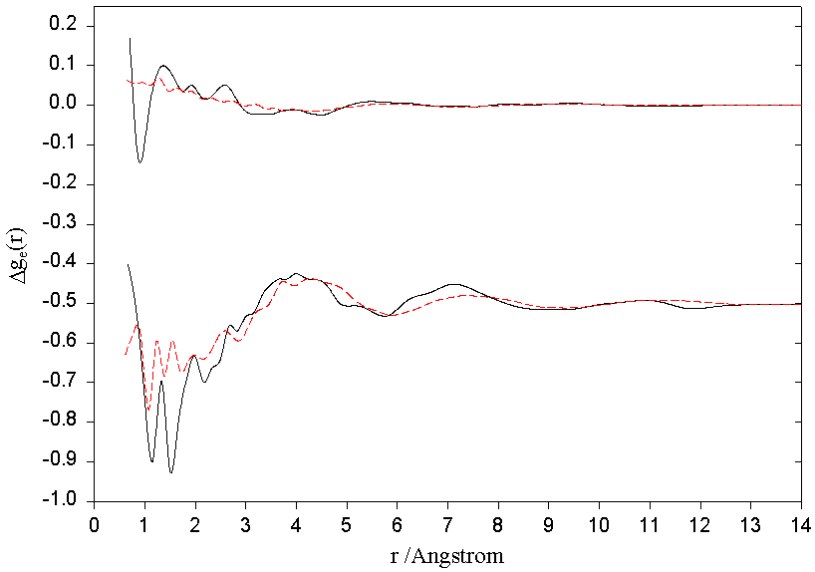

Figure 11. Lower curves (displaced by −0.5 units): electronic isotopic difference CD_3OD–CH_3OH at −80 °C (solid line) is compared to the difference: {CH_3OH at −80 °C–CH_3OH at 24.5 °C}/3 (dashed line). Upper curves: electronic isotopic difference CD_3OD–CD_3OH at −30 °C (solid line) is compared to the difference: {CD_3OH at −24.5 °C–CD_3OH at −30 °C}/10 (dashed line).

(figure 5) for both forms of the methyl substitution. At −80 °C it appears that the CD_3OH has a significantly shorter O–O nearest-neighbour distance than CH_3OH. The CD_3OD–CH_3OH difference shows a broad peak just below 2.8 Å, indicating that the CD_3OD O–O nearest neighbour distance is slightly longer. The increased strength of the isotopic effects compared with the same differences at room temperature can be understood in terms of the increasing importance of ground state quantum librations as temperature is lowered.

In figure 10, the hydroxyl substitution differences are shown to be much smaller than those in figure 9 at intermolecular distances. As was shown in paper I, the hydroxyl effect is far less significant than the methyl effect at this temperature. As was seen for these differences at room temperature, the main intermolecular effect is a broad peak at the 2.8 Å which is due to H-bonding. This feature is approximately the same size relative to the total structure as at room temperature. The associated carbon feature near 3.8 Å is not visible, perhaps due to poorer statistics. At intramolecular distances, the effect is similar in size to the differences at room temperature.

Figure 11 compares isotopic differences at −30 and −80 °C with structural differences induced by scaled temperature changes of 5.5 and 35 °C respectively. Fully deuterating CH_3OH at −80 °C is shown to correspond to cooling it by about 35 °C while deuterating at the hydroxyl site in CD_3OH at −30 °C corresponds to warming it by 5.5 °C. The electronic structures are shown (using equation (4) to transform) because the pseudonuclear structure derived using equation (5) did not obtain such good agreement. The reasons for this are unknown, but it may be due to the fact that the former is measured while the latter involves an assumption about the electronic structure (the IAA). The good agreement of the electronic isotopic differences to the electronic temperature difference shows that temperature shifts will correct out the differences in electronic structure between two isotopic samples. Further refinements may be necessary to apply this technique to pseudonculear differences.

The densities of methanol at −80 and −30 °C were estimated by comparing normalization constant of the same sample in the same tube for each isotope. It is assumed that all four isotopes increase by the same ratio in going from 25 to −80 °C giving a mean {density at −80 °C}/{density at RT} ratio of 1.079 over the four isotopes. This yields a molecular density of 0.0161 molecules $Å^{-3}$ for methanol at −80 °C. This agrees well with an extrapolation from thermodynamic data [13] which yields the same value.

5. Conclusions

The room temperature methanol results show clearly that the quantum effects originate from both differences in the librational motion and differences in the winding hydrogen-bonded chain structure of each isotopic liquid. The maximum isotopic effects range from 2 to 10% of the total structure depending on the isotopic difference and the temperature.

There are clear changes in the nearest-neighbour H-bonding lengths that are due to perturbations in the H-bond caused by mass effects. Effects caused by isotopic differences in molecular librations are apparent, in the form of sharpened peaks for certain isotopes. At intramolecular distances, the heavier isotope exhibited sharper peaks, as expected from its decreased quantum motions. However, at larger distances the behaviour was more complex, especially near the characteristic O–O nearest-neighbour distance. The heavier isotope had a sharper 2.8 Å peak for hydroxyl substitutions, as expected, but this peak was less sharp for the heavier isotope in methyl substitutions.

The two substitution sites produce opposing effects in Q-space (see paper I) so it is not surprising that opposing effects are also observed in r-space. However, it is unclear why heavier isotopes in hydroxyl (rather than the methyl) substitutions produced sharper peaks at 2.8 Å. It is also surprising that the hydroxyl substitution that produced this sharpening corresponded to heating the liquid by 4 °C (rather than the expected cooling) in Q-space. One possible explanation is that broadening of features at other distances produced a compensating heating effect in the hydroxyl substitutions. However, further experimental and simulation studies are required to understand these observations.

Our measured temperature derivatives are able to duplicate these effects for the electronic structure in real space as was seen in paper I for Q-space. This fact can be used in conjunction with isotopic substitution measurement [14] to correct partial structure measurements for quantum effects [15]. The poorer agreement obtained when the comparisons between isotopic differences and temperature derivatives are made using pseudonuclear data indicates the limitation of this method when applied to data other than the electronic structure.

These experiments have shown clearly measurable influences upon liquid structure caused by the quantum effects in methanol, which vary with temperature and molecular group. They set clear limits on the accuracy of widely used H/D substitution techniques in neutron diffraction and suggest a method of compensating for isotopic effects in future experiments employing H/D substitution by making appropriate temperature shifts between different samples.

Acknowledgments

Staff at the Hamburger Synchrotronstrahlungslabor HASYLAB and the European Synchrotron Radiation Facility ESRF are thanked for providing the apparatus and the beamtime, and their assistance in conducting the experiments. Professor A K Soper is thanked for many useful discussions concerning the x-ray data. The work of the Canadian participants was supported by a grant from NSERC Canada. This work was performed in part under contract no W-31-109-ENG-38 with the US Department of Energy.

References

[1] Benmore C J and Egelstaff P A 1996 *J. Phys.: Condens. Matter* **8** 9429–32
[2] Kuharski R A and Rossky P J 1985 *J. Chem. Phys.* **82** 5164
[3] Del Buono G S, Rossky P J and Schnitker J 1991 *J. Chem. Phys.* **95** 3728–37
[4] Sesé L M 1996 *Mol. Phys.* **89** 1783–802
[5] Root J H, Egelstaff P A and Hime A 1986 *Chem. Phys.* **109** 5164
[6] Tomberli B, Benmore C J, Egelstaff P A, Neuefeind J and Honkimäki V 2000 *J. Phys.: Condens. Matter* **12** 2597–616
[7] Tomberli B, Benmore C J, Egelstaff P A, Neuefeind J and Honkimäki V 2001 Temperature dependence of structural quantum effects in liquid methanol *Europhys. Lett.* **51** 341–7
[8] Benmore C J, Tomberli B, Egelstaff P A and Neuefeind J 2001 *Mol. Phys.* **99** 787–94
[9] Hubbell J H, Veigele W J, Briggs E A and Howerton R J 1973 *J. Phys. Chem. Ref. Data* **4** 471
[10] Narten A H and Habenschuss A 1984 *J. Chem. Phys.* **80** 3387
[11] Magini M, Paschina G and Piccaluga G 1982 *J. Chem. Phys.* **77** 2051–6
[12] Ludwig R and Weinhold F 2000 *Phys. Chem. Chem. Phys.* **2** 1613
[13] Bhattacharyya D and Thodos G 1964 *J. Chem. Eng. Data* **9** 530
[14] Yamaguchi T, Hidaka K and Soper A K 1999 *Mol. Phys.* **96** 1159
[15] Benmore C J, Tomberli B, Neuefeind J and Egelstaff P 2001 *J. Appl. Phys.—Int. Conf. Neutron Scattering 2001* at press